Applied Thermal Engineering 139 (2018) 542–551

Contents lists available at ScienceDirect

Applied Thermal Engineering

journal homepage: www.elsevier.com/locate/apthermeng

Research Paper

Temperature distribution measurements and modelling of a liquid-liquid-vapour spray column direct contact heat exchanger

Ali Sh. Baqir[a], Hameed B. Mahood[b,*], Asaad H. Sayer[c]

[a] Department of Aeronautical Engineering, Engineering Technical College- Najaf, Al-Furat Al-Awsat Technical University, 31001 Al- Najaf, Iraq
[b] University of Misan, Misan, Iraq
[c] University of Thi-Qar, College of Science, Chemistry Department, Thi-Qar, Iraq

HIGHLIGHTS

- Measurements and calculation of T_c and T_d along 3-phase spray column DCHE.
- Effect of Q_c,Q_d,D_{nz},ja and sparger configuration was examined.
- T_c decreases with Z, whilt T_d increases.
- $T_{c\ out}$ increases with increasing continuous phase flow rates.
- $T_{c\ out}$ decreases with increasing dispersed phase flow rates.
- $T_{c\ out}$ increases with increasing Ja.

ARTICLE INFO

Keywords:
Direct contact heat transfer
Direct contact evaporator
Experimental technique
Modelling
Temperature distribution

ABSTRACT

This study investigates the temperature distribution of a liquid-liquid-vapour three-phase direct contact heat exchanger, both experimentally and theoretically. The experimental investigation was conducted using a Perspex column with an internal diameter of 10 cm and 100 cm height. Liquid pentane at its saturation temperature and warm water were used in the dispersed phase and continuous phase respectively. Various dispersed phase flow rates (10,15 & 20 L/h) and continuous phase flow rates (10,20,30 & 40 L/h) were tested using three different sparger configurations (7,19 & 36 nozzles) and two different nozzle diameters (1 & 1.25 mm). The results showed that the temperature of the continuous phase decreased with the height of the heat exchanger from its inlet at the top towards its outlet at the bottom. This behaviour was entirely opposite to the dispersed phase that flows counter currently with the continuous phase in the heat exchanger. For the same sparger and constant continuous phase flow rate (Q_c), the outlet temperature of the continuous phase was inversely affected by the dispersed phase flow rate (Q_d); while decreasing the nozzle numbers in the sparger led to a decrease in the outlet temperature of the continuous phase. Furthermore, the initial temperature of the continuous phase in terms of the Jakobs number (Ja) was found to have a significant positive impact on outlet temperature: the higher the Ja, the higher the outlet temperature. The analytical model had an acceptable agreement with the experimental measurements.

1. Introduction

The increase in global population and industrialisation, and hence the growth of cities, has steadily increased the demand for energy everywhere, and this increase presents a real challenge for civilization. The development of new sustainable alternative technologies such as wind and solar energy, along with the enhancement of energy conversion cycles, could offer practical solutions for such problems [1,2]. In this context, there is no doubt that direct contact heat exchangers are likely to be the appropriate choice. The absence of internals or barriers between the contacting fluids means that direct contact heat exchangers have many advantages over surface type heat exchangers such as the shell and tube. These surfaces or barriers can be exposed to fouling, corrosion and thermal stresses, particularly when used in a high temperature range. Such problems are alleviated by different technologies, for example by using chemicals as a corrosion inhibitor, which raises operational costs and may require expensive special construction materials. This can, of course, hinder the applicability of surface type heat

* Corresponding author.
E-mail address: hbmahood@yahoo.com (H.B. Mahood).

https://doi.org/10.1016/j.applthermaleng.2018.04.128
Received 2 November 2017; Received in revised form 10 March 2018; Accepted 26 April 2018
Available online 28 April 2018
1359-4311/

Nomenclature

A_c	condenser cross-sectional area (m^2)
A_i	heat transfer area (m^2)
a	radius of two-phase bubble (m)
a_o	initial radius of two-phase bubble (m)
C_{pc}	specific heat of continuous phase (kJ/kg K)
C_{pd}	specific heat of dispersed phase (kJ/kg K)
D	the two-phase bubble diameter (m)
D_{nz}	Nozzles' diameters (mm)
D_o	initial drop diameter (m)
$f(Z)$	function appears in Eq. (20)
Ja	Jacobs number ($\rho_c C_{pc} \Delta T / \rho_v h_{fg}$)
H_c	enthalpies of the continuous phase (J/kg)
H_{dl}	enthalpy of dispersed liquid phase (kJ/kg)
H_{dt}	total enthalpies of the dispersed phases (J/kg)
H_{dv}	enthalpy of dispersed vapour phase (kJ/kg)
h	heat transfer coefficient (W/m^2 K)
h_{fg}	latent heat of vaporization (kJ/kg)
k	thermal conductivity of the continuous phase (W/m K)
k_v	velocity factor
$\dot{m}_c$	mass flow rate of continuous phase (kg/s)
$\dot{m}_d$	mass flow rate of dispersed phase (kg/s)
Nu	Nusselt number ($2ah/k_c$)
nz	number of nozzles in the sparager
Pe	Peclet number ($2a_o U_o/\epsilon$)
Pr	Prandtl number ($C_{pc}\mu_c/k_c$)
Q	heat transfer rate (W)
Q_c	volumetric flow rate of continuous phase (L/h)
Q_d	volumetric flow rate of dispersed phase (L/h)
T_c	temperature of continuous phase (°C)
$T_{c\ out}$	outlet temperature of the continuous phase (°C)
T_d	temperature of dispersed phase (°C)
ΔT	temperature difference (°C)
U_c	velocity of the continuous phase (m/s)
U_d	velocity of the dispersed phase (m/s)
U_o	initial velocity of the dispersed phase (m/s)
V	volume (m^3)
x	vaporization ratio
Z	height (m)

Greek samples

μ_c	viscosity of the continuous phase (N s/m^2)
ρ_c	density of the continuous phase (kg/m^3)
ρ_d	density of the dispersed phase (kg/m^3)
ρ_{dl}	density of the dispersed liquid phase (kg/m^3)
ρ_{dv}	density of the dispersed vapour phase (kg/m^3)
ϵ	thermal diffusivity (m^2/s)
ϕ	volume fraction

exchangers in low-temperature processes. Moreover, other challenges such as high initial and operational costs are encountered in the selection and operation of conventional heat exchangers. The high initial costs result from the large surface area which is essential to overcome the low heat transfer rate or heat transfer coefficient, while the high operational costs are mainly due to the expense of continuous maintenance to combat fouling and corrosion. These problems and others can be avoided by the use of direct contact heat exchangers. The advantages of these exchangers include a high heat transfer coefficient, simple design, low costs, and negligible fouling and corrosion problems, enabling high efficiency to be achieved. Therefore, direct contact heat exchangers can potentially be used in fields where surface type heat exchangers cannot [3].

Direct contact heat exchangers, and in particular three-phase spray column direct contact heat exchangers, are based on the heat transfer between a continuous phase (using liquid) and a dispersed phase (using liquid drops or vapour bubbles). The temperature of the continuous phase is greater or less than the saturation temperature of the drops or bubbles, depending on whether the process of evaporation or condensation respectively is being used. The dispersed phase therefore undergoes a change of its phase, and a high heat rate will be absorbed or liberated depending on the process.

The heat transfer mechanism during the evaporation of a drop in direct contact with another immiscible liquid has not been understood entirely, although considerable attention has been devoted to the subject. This mechanism was first investigated during the 1960s and has since been the subject of a number of different studies. It has been suggested that the mechanism has many possible uses, including in water desalination by freezing [4], heat recovery systems [5], ice-slurry production [6] and thermal energy storage [7]. Nevertheless, the scientific literature lacks studies of three-phase direct contact heat exchangers.

The aim of using the direct evaporation process is to extract the maximum energy from that available in the hot or continuous fluid by heating up and vaporising the dispersed fluid. The best way to evaluate this process is to measure the dispersed phase and continuous phase temperatures along the heat exchanger. Similarly, experimental and theoretical studies have investigated the temperature distribution along the height of a spray column direct contact heat exchanger. Most of these theoretical investigations were based on numerical models, since analytical solutions are quite difficult to obtain [8–16]. Battya et al. [8] theoretically investigated (numerically) the temperature distribution of both the continuous and dispersed phases along the direct contact evaporator. Runge–Kutta method was used to perform the analysis with the assumption of a constant volumetric heat transfer coefficient. The temperature distribution of both phases (continuous and dispersed) along the spray column direct contact evaporator was calculated for different dispersion coefficients. The maximum divergence from the experimental data was about 9%. Similarly, and separately, Cabon and Boehm [9], Jacobs and Golafshani [10], Core and Mulligan [11], and Summers and Crowe [12] predicted numerically the temperature distribution of the dispersed and the continuous phase along three-phase direct contact evaporator height. Their numerical results were compared with experimental data.

Tadrist et al. [13] carried out experimental measurements and developed a numerical model including the coalescence of the evaporating drops for temperature distribution and holdup ratio in the three-phase direct contact spray column evaporator.

Brickman and Boehm [14] solved numerically utilising the Rung-Kutta technique the one-dimensional, continuity, momentum and energy equations. Their numerical model concentrated on the capability of maximising the output of a three-phase, direct contact heat exchanger as well as the prediction of the temperature distribution of both phases along the heat exchanger. The Birkman and Boehm [14] results indicated that the optimal performance can be achieved only when the dispersed phase is injected at its saturation temperature. Mahood et al. [15] measured experimentally and modelled analytically the temperature distribution of the continuous phase and dispersed phase along a short direct contact condenser. Different operational parameters, such as the initial temperature of the dispersed phase, and the flow rate of both phases were investigated. Mahood et al. [16] investigated analytically the temperature distribution along the three-phase direct contact heat exchanger under a wide range of the operational parameters. Their results were compared successfully with experimental data with a

maximum divergence of about 12%.

Recently, attention has been directed to studying, both experimentally and theoretically, the heat transfer performance of the three-phase direct contact heat exchanger [1,2,17–23]. These studies have involved innovative models for the hydrodynamics of a bubble swarm during evaporation or condensation in direct contact with immiscible liquids [24,25].

It is obvious that all previous studies were concerned with theoretical models, most specifically, numerical models. In addition to, these studies have ignored the effect of sparger configuration on the hydrodynamics and heat transfer in the three-phase direct contact heat exchanger. This parameter was found to be having a significant impact on the heat transfer process and hence on the output of the three-phase direct contact heat exchanger [1]. However, a fully understanding of the heat transfers mechanism of the three-phase direct contact heat exchanger is rare and required more attention towards developing designable correlations or analytical models.

To full the gab, in the present study, the temperature distribution of the liquid-liquid-vapour spray column direct contact heat exchanger was examined experimentally and modelled analytically. Many parameters were studied, such the continuous phase flow rate, the dispersed phase flow rate, the temperature driving force in terms of Ja, and the sparger configuration, and their effects on both the temperature distribution along the exchanger and the continuous phase outlet temperature. An analytical model based on the previous study by Mahood et al. [15] was developed for this study to predict the temperature distribution along the heat exchanger.

2. Experimental work

2.1. Experimental setup

Fig. 1 shows the schematic of the apparatus used in the present study. The apparatus is comprised of the direct contact heat exchanger test section part, the continuous phase supply part, the dispersed phase supply part, measuring devices and data acquisition. The test section part consists of a Perspex cylindrical tube of 100 cm height and 10 cm internal diameter, a sparger and rotameters. Eighteen holes of equal size were made in the Perspex tube to enable the thermocouples to be affixed. The test section was connected to the continuous phase inlet tube at the top, and to the dispersed phase injection at the bottom via a sparger. The continuous phase supply system included a large (500 L) constant temperature water bath with a controller, continuous phase storage tank, water pump, pipes, fittings and valves. The water bath was heated by three electrical heaters (3 kW each). In addition, a safety valve of 1.5 bar operating pressure was used to control the pressure in the water bath. Distilled water was used as the continuous phase fluid. It was supplied from a large storage tank (500 L) via copper tubing, and was heated to the required temperature using a copper coil of 10 mm outer diameter and 2.5 m long. The copper coil was entirely immersed in the constant temperature water bath. A peristaltic pump (50 L/h maximum flow rate) was used to feed the water to the test section via a 4.8 mm inside diameter silicone tube. The flow rate before it entered the test section was measured using a rotameter with an inaccuracy of ± 1.5%.

The dispersed phase supply system comprised a 20 L capacity plastic storage tank, peristaltic pump, pipes, valves, rotameter and fittings. Liquid pentane (99% purity) was used. The initial temperature and flow rate of the dispersed phase were measured just before the injection into the test section using a calibrated thermocouple (±1% in acuracy) and rotameter (±1.5 maximum in accuracy), respectively.

The experiment used 18 calibrated K-type thermocouples to measure the temperature distribution along the test section, and the inlet and outlet temperatures of the continuous phase and dispersed phase (see Fig. 1b). These thermocouples were connected to a digital data logger which was connected to a PC. Finally, the dispersed phase vapour produced at the top of the test section was condensed and returned to the liquid pentane storage tank by utilising a surface type condenser.

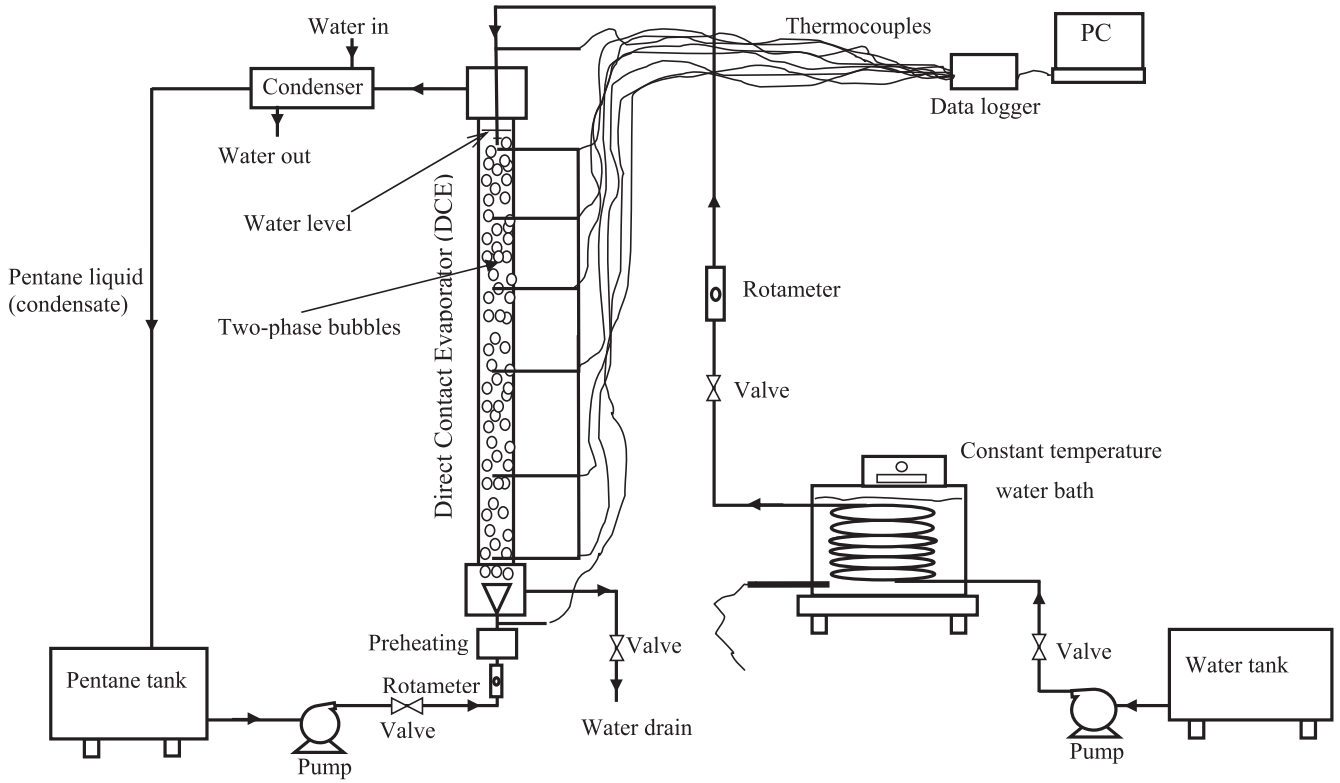

Fig. 1a. Schematic diagram of the experimental rig.

2.2. The experimental procedure

The temperature distribution along the three-phase spray column direct contact heat exchanger was measured utilising the experimental unit (Fig. 1a) and was also calculated using the developed analytical model. Each experiment began by filling the continuous phase water bath with distilled water and then heating it to the desired temperature. This hot water was circulated throughout the test section and was maintained at a constant temperature and height. The continuous phase flow rate was then determined. The desired flow rate of the dispersed phase was injected into the test section as small drops by passing it via the sparger. Three different sparger configurations (7, 19 and 36 nozzles) were used in the experiments. Fig. 2 shows the sparger configurations. When the dispersed phase drops were injected, the temperature of the continuous phase (hot distilled water) was measured along the test section, and was found to decrease from the inlet point at the top towards the outlet at the bottom. The reason for this decrease is that the cool drops from the dispersed phase absorb heat from the hotter continuous phase, heat up, evaporate along the test section and finally completely vaporise at the top of the test section. Therefore, two-phase (liquid/vapour) bubbles are formed and are seen throughout the entire height of the test section.

Only the inlet and outlet temperatures of dispersed phase were measured in the experiments. All measurements were displayed directly on the PC via the data logger, and the steady state results were collected when the experiment reached steady conditions.

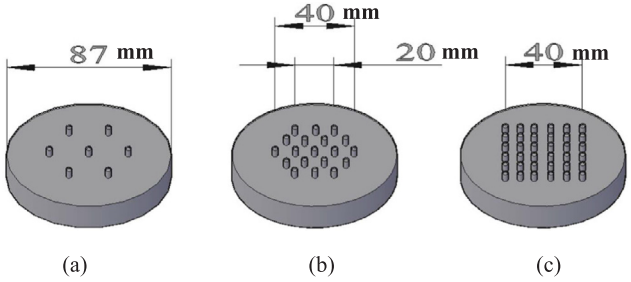

Fig. 2. Sparger configurations with (a) 7 holes, (b) 19 nozzles and (c) 36 nozzles.

3. Modelling

A simple analytical model based on one previously developed by Mahood et al. [15] was developed. However, in contrast to the previous model, the new model introduced the effect of latent heat on the direct contact heat transfer process.

The one-dimensional flow model can be assumed to be accurate because of the small bubbles in comparison with the heat exchanger diameter and with the assumption of non-circulation zones inside the heat exchanger [9,10]. In addition, the flow rate of each phase can be assumed to be constant along the test section, because of the immiscibility between the two phases.

However, the continuity equations for the counter-current flow of the two phases can be expressed as:

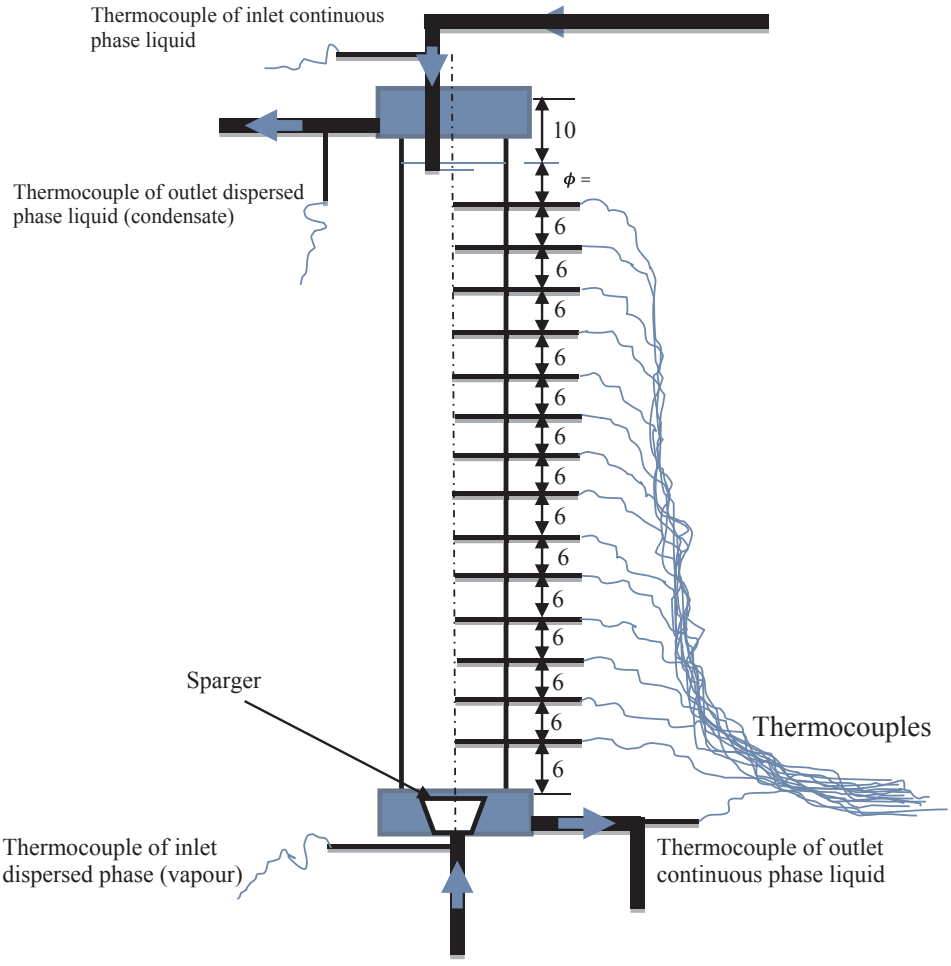

Fig. 1b. Thermocouples distribution over the test section.

$$\dot{m}_d = \rho_d A_c \phi U_d \tag{1}$$

and

$$\dot{m}_c = \rho_c A_c (1-\phi) U_c \tag{2}$$

where A_c represents the evaporator cross-sectional area.

For one-dimensional, steady-state flow, the energy equations for the two phases can be written as:

$$\frac{d}{dZ}[\rho_c(1-\phi)U_c H_c] = -\frac{Q}{V} \tag{3}$$

and

$$\frac{d}{dZ}[\rho_d \phi U_d H_{dt}] = \frac{Q}{V} \tag{4}$$

Substituting Eqs. (1) and (2) in Eqs. (3) and (4) respectively, where there is no heat loss to the surrounding, yields:

$$\frac{dH_c}{dZ} = \frac{-A_c}{\dot{m}_c}\frac{Q}{V} \tag{5}$$

and

$$\frac{dH_{dt}}{dZ} = \frac{A_c}{\dot{m}_d}\frac{Q}{V} \tag{6}$$

Here Q represents the total heat transfer from the continuous phase to the dispersed phase. Hence;

$$Q = hA_i\Delta T \tag{7}$$

where A_i and ΔT denote the heat transfer area and the temperature driving force respectively.

The enthalpies of the continuous and the dispersed phases, H_c and H_{dt} which appear in Eqs. (3) and (4) can be found using the following expressions respectively:

$$H_c = C_{pc} T_c \tag{8}$$

and

$$H_{dt} = C_{pd} T_d + xH_{dv} + (1-x)H_{dl} \tag{9}$$

Substituting Eqs. (7)–(9) into Eqs. (5) and (6) respectively, results in:

$$\frac{dT_c}{dZ} = -\frac{h\Delta T A_c}{\dot{m}_c C_{pc}}\left(\frac{A_i}{V}\right) \tag{10}$$

and

$$\frac{dT_d}{dZ} = \left(\frac{h\Delta T A_c}{C_{pd}\dot{m}_d}\right)\left(\frac{A_i}{V}\right) + \left(\frac{h_{fg}}{C_{pd}}\right)\frac{dx}{dZ} \tag{11}$$

The interfacial area per unit volume $\left(\frac{A_i}{V}\right)$, which appears in Eqs. (10) and (11) can be given as:

$$\left(\frac{A_i}{V}\right) = \frac{6\phi}{D} \tag{12}$$

where D denotes the two-phase bubble diameter ($D = 2a$). It can be found using the expression given by [26] as:

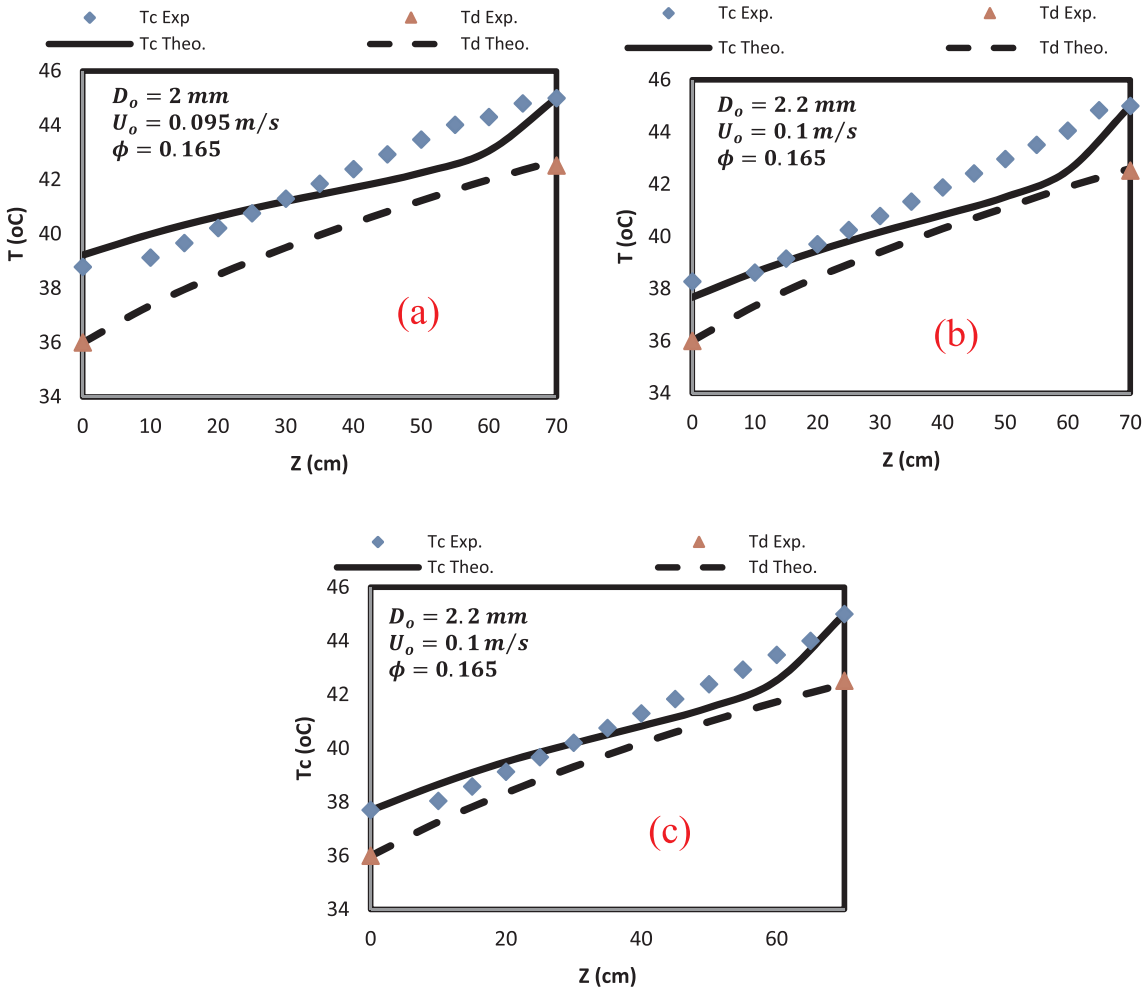

Fig. 3. The temperature distribution of both the continuous and dispersed phases along the direct contact heat exchanger height for Q_d = 10 L/h and D_{nz} = 1 mm for (a) Q_c = 40 L/h (b) Q_c = 30 L/h and (c) Q_c = 20 L/h.

$$a = a_o\left(1 + x\left(\frac{\rho_{dl}}{\rho_{dv}} - 1\right)\right)^{1/3} \tag{13}$$

where x,ρ_{dl} and ρ_{dv} represent the vaporization ratio, the continuous phase liquid density and the dispersed phase vapour density, respectively.

The final forms of the temperature distribution equations, now become:

$$\frac{dT_c}{dZ} = \left(-\frac{3\phi}{a}\right)\left(\frac{h\Delta TA_c}{C_{pc}\dot{m}_c}\right) \tag{14}$$

and

$$\frac{dT_d}{dZ} = \left(\frac{3\phi}{a}\right)\left(\frac{h\Delta A_c}{C_{pd}\dot{m}_d}\right) + \left(\frac{h_{fg}}{C_{pd}}\right)\frac{dx}{dZ} \tag{15}$$

Utilising the similarity of the concentric spheres model and the cell model which has been used successfully by [3], a modified equation for the heat transfer coefficient in terms of Nu was obtained. This equation is valid for the case of multi-drops/bubbles evaporation or condensation in direct contact with another immiscible liquid, given as:

$$Nu = \frac{0.6308}{\sqrt{1-\phi}}Pe^{0.5} \tag{16}$$

where

$$Nu = \frac{2ah}{k} \tag{17}$$

Eq. (16) was derived using the potential flow assumption around the two-phase bubble. Because of the absence of a real or viscous solution for the evaporation of the two-phase bubble to compare with the potential flow solution, [15,27–29] used the flowing velocity factor, in which the solution is based on the assumption that the potential flow is converted to an actual, or viscous solution, giving:

$$k_v = 0.25Pr^{-\frac{1}{3}} \tag{18}$$

where $Pr = \mu_c C_{pc}/k$ is the Prandtl number.

And for pure potential flow $k_v = 1$.

Finally, the progress of the evaporation along the direct contact evaporator represented by $\frac{dx}{dz}$ can be obtained for simplicity by fitting the experimental data as $f(Z)$ of [30]. Substituting Eqs. (16) and (17) into Eqs. (14) and (15), integrating the results, and assuming that the two-phase bubble is a constant and is equal to its initial radius [10,16] [results in:

$$T_c = T_{co} - \left[(0.946)\left(\frac{U_o k_v}{\epsilon}\right)^{0.5}\left(\frac{k_c \Delta TA_c}{C_{pc}\dot{m}_c a_o}\right)\left(\frac{\phi(1-\phi)}{(\phi + 0.5)^{0.5}}\right).Z\right] \tag{19}$$

and

$$T_d = T_{do} + \left\{\left[\left[(0.946)\left(\frac{U_o k_v}{\epsilon}\right)^{0.5}\left(\frac{k_c \Delta TA_c}{C_{pd}\dot{m}_d a_o}\right)\left(\frac{\phi(1-\phi)}{(\phi + 0.5)^{0.5}}\right).Z\right] + \left(\frac{h_{fg}}{C_{pd}}\int_0^Z f(Z)dZ\right)\right]\right\} \tag{20}$$

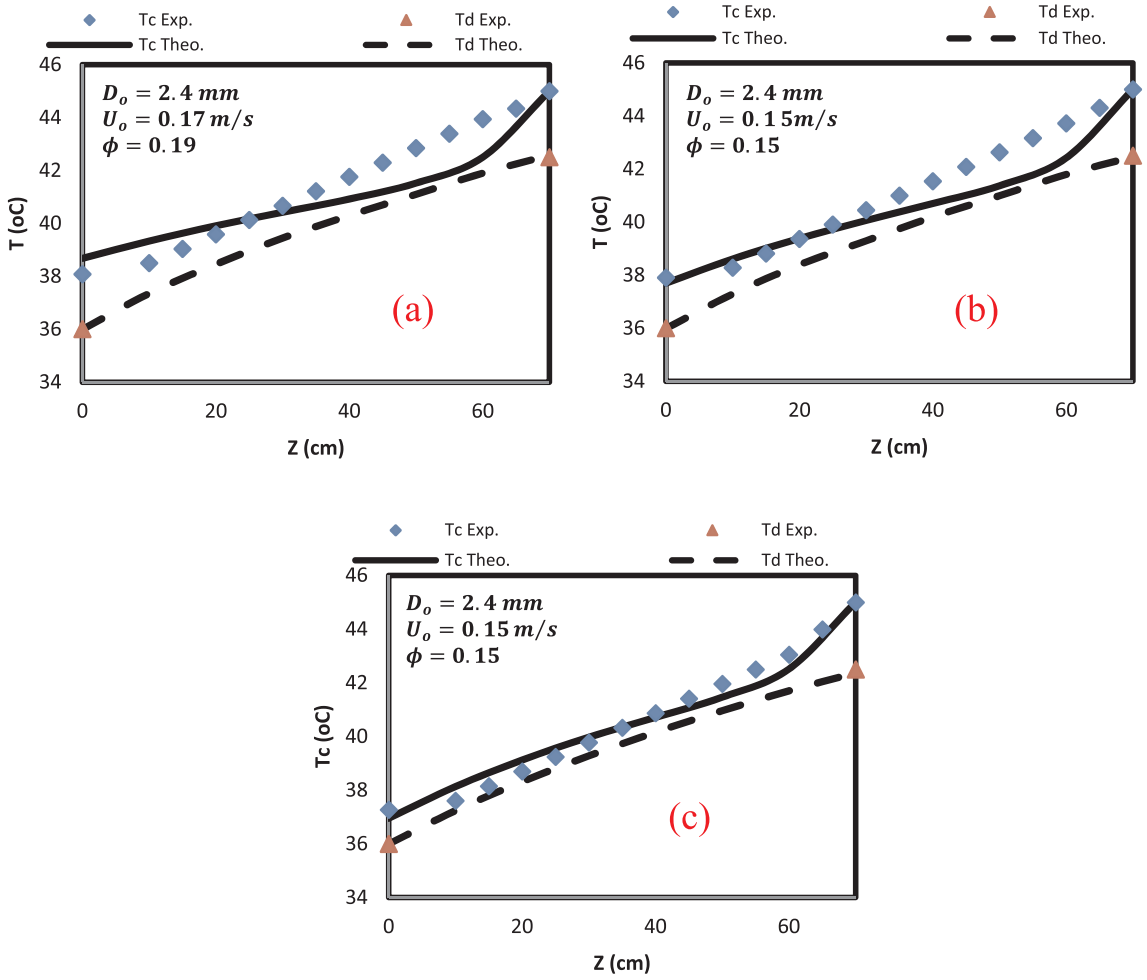

Fig. 4. The temperature distribution of both the continuous and dispersed phases along the direct contact heat exchanger height for Q_d = 15 L/h and D_{nz} = 1 mm for (a) Q_c = 40 L/h (b) Q_c = 30 L/h and (c) Q_c = 20 L/h.

4. Results and discussion

The aim of the present study is to investigate experimentally and theoretically the temperature distribution of the continuous phase and dispersed phase along a direct contact heat exchanger. Due to the difficulty of measuring the dispersed phase temperature at different points along the heat exchanger, only the dispersed phase inlet and outlet temperatures were measured in the experiments. However, the dispersed phase temperature distribution was predicted by the analytical model after the model validation.

To conduct the temperature measurements 18 calibrated K-type thermocouples were fixed at equal distances along the heat exchanger. A sample of the direct measurements of these thermocouples at steady state conditions along the heat exchanger is shown in Figs. 3–5 for three different continuous phase flow rates (Q_c = 40,30 and 20 L/h), two dispersed phase flow rates (Q_d = 10 and 15 L/h) and two different nozzle diameters (D_{nz} = 1 and 1.25 mm). In addition, the figures include the results of the analytical model calculated using Eqs. (19) and (20). The temperature of the continuous phase decreases with height, being at its highest at the inlet at the top of the heat exchanger, and at its lowest at the drainage point at the bottom. This behaviour is almost linear, except in the upper and lower parts of the heat exchanger. This could be attributed to the fact that the fluid reaches the lower part of the heat exchanger with high energy content, while the dispersed phase two-phase (liquid/vapour) bubbles remain almost liquid, nearly at their saturation temperature: consistently, the internal heat transfer resistance, which controls the direct contact heat exchange process, remains at its lowest value. Furthermore, the temperature difference (which represents the driving force for evaporation) between the contacting fluids is the largest at the lowest part (bottom) of the heat exchanger. Consequently, a highly convective heat transfer between the contacting two-phase fluids takes place here. A large amount of the thermal energy of the continuous phase is absorbed by the non-vaporised dispersed drops, resulting in a significant reduction in the continuous phase temperature. Nevertheless, the outlet temperatures of the dispersed phase seem independent on the initial temperature of the continuous phase (see Table 1) which clearly indicates that the direct contact heat transfer process is a latent heat dominant process. This completely agreed with our knowledge of heat transfer process associates with a phase change.

Unfortunately, technical difficulties prevented measurement of the

Table 1
The outlet temperatures of both phases (dispersed and continuous phase) at different operational conditions.

Q_c (L/h)	T_{do} (°C)				T_{co} (°C)			
	Q_d (L/h):	10	15	20	Q_d (L/h):	10	15	20
10		42.43	42.36	42.36		37.36	37.00	36.75
20		42.46	42.40	42.51		38.12	37.66	37.24
30		42.39	42.50	42.44		38.39	38.34	37.68
40		42.55	42.42	42.51		39.21	38.90	37.99

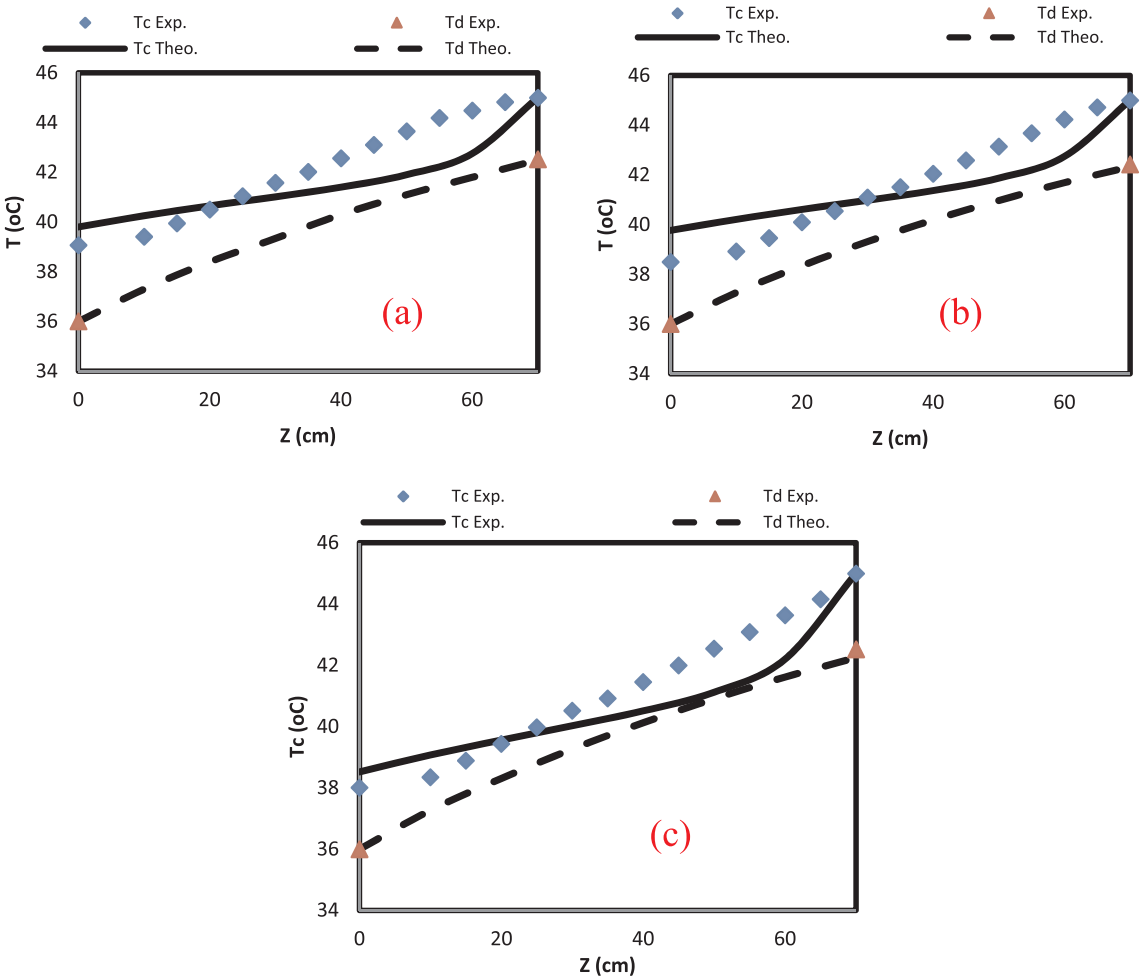

Fig. 5. The temperature distribution of both the continuous and dispersed phases along the direct contact heat exchanger height for Q_d = 10 L/h and D_{nz} = 1.25 mm for (a) Q_c = 40 L/h (b) Q_c = 30 L/h and (c) Q_c = 20 L/h.

temperature of the dispersed phase along the heat exchanger. The dispersed phase temperature was measured only at the injection and outlet points, as already mentioned. Therefore, a pure linear behaviour along the heat exchanger has been predicted and appears in the figures. However, the behaviour of the temperature of the dispersed phase should be more accurately predicted by the analytical model. It is apparent from the figures that the temperature of the dispersed phase has a clear non-linear trend along the heat exchanger.

Furthermore, Figs. 3 and 4 show the validation of the present analytical model by comprising its results with the experimental measurements. However, the model was developed in based on one-dimensional mass and energy equations. All the necessary input parameters, such as the drops initial diameters, hold-up and initial drops velocity has been selected from the experimental measurements. As shown by Figs. 3–5, the simple model can fit acceptably the experimental data. The average relative divergence between the two sets of results was about 10%. The model was noticed to having a high sensitivity to the change in both the hold-up and the initial diameters of the drops. Both of these effective parameters were measured during the experiments using a high-speed camera and the change in the continuous phase level, respectively. In general, the model's results divergence from the experimental data was near the top region of the column. This could be due to the complex fluid mechanics and heat transfer phenomena that occurred in this part of heat exchanger. The drops through this part of the column, are almost all vapour and hence the heat resistance at its maximum value. Nevertheless, drops break down or defragment and coalesces is highly capable in this region. However, the simple analytical model, which excluded such complex fluid dynamics phenomena, is expected to poorly fit the experimental data.

The variation of the continuous phase outlet temperature under different operational conditions is shown in Fig. 6. Three different sparger configurations (different number and constant diameter of nozzles) and two dispersed phase flow rates are examined in this figure. It is apparent that the lowest number of nozzles in the sparger results in the lowest outlet temperature in the continuous phase. At a constant flow rate and at the initial temperature, a large number of injection nozzles in the sparger results in the production of large drops because of low injection pressure and hence velocity (long drop formation time). The initial drops size formed at a nozzle is proportional inversely with the injecting velocity. The higher the injection velocity, the lower the drops size is. Consequently, the interfacial heat transfer area, which is the most effective factor, is reduced (in case of large drops) according to Eq. (12). Consistently, the heat transfer rate and volumetric heat transfer coefficient are reduced as well [23]. Therefore, the amount of energy absorbed by the dispersed phase as a result of the direct contact heat transfer is small. Accordingly, the continuous phase leaves the heat exchanger with high energy content or a high temperature.

In addition, Fig. 6 illustrates the effect of the dispersed phase flow rate on the outlet temperature of the continuous phase. Apparently, the higher the flow rate of the dispersed phase, the lower the outlet temperature of the continuous phase. This could be attributed to the fact that a high dispersed phase flow rate results in the absorption of almost all the dispersed phase heat and hence a reduction in outlet temperature. Furthermore, the number of nozzles in the sparger results in enhancing the direct contact evaporation process [1,23]. This is because the production of small droplets increases the interfacial heat transfer area; consequently, the continuous phase flow rate required for evaporating the same dispersed phase flow rate is lower. This fact is shown in Fig. 6, since at a constant dispersed phase flow rate, an increase in the number of injecting nozzles results in an increase of the continuous phase outlet temperature. This result is of practical significance, as it is possible to considerably reduce the flow rates of the contacting fluids by increasing the number of injection nozzles in the sparger. This will have a positive impact on pumping costs and therefore minimises the cost of the process.

Similar behaviour was observed in the case of the effect of nozzle diameter on continuous phase outlet temperature, and this is shown in Fig. 7. It is apparent that the smallest nozzle diameter results in a reduction in the continuous phase outlet temperature. The reasons for this could be similar to those mentioned in the discussion of Fig. 6. A larger nozzle diameter produces a large drop size, as a result of reducing the injection velocity of the dispersed phase. Consequently, the associated interfacial heat transfer area between the contacting phases is reduced and so the heat transfer will be smaller. The continuous phase will leave the heat exchanger with a higher temperature. Once again it is obvious that the higher the dispersed phase, the lower the continuous phase outlet temperature. This is entirely consistent with the results shown in Fig. 6. However, the reliance of the continuous phase outlet temperature on the dispersed phase flow rate is shown quantitatively in Fig. 8 for two different continuous phase flow rates and three different sparger configurations. As previously mentioned, the outlet temperature of the continuous phase decreases with the increase in the dispersed phase flow rate, and with the decrease in the number of nozzles

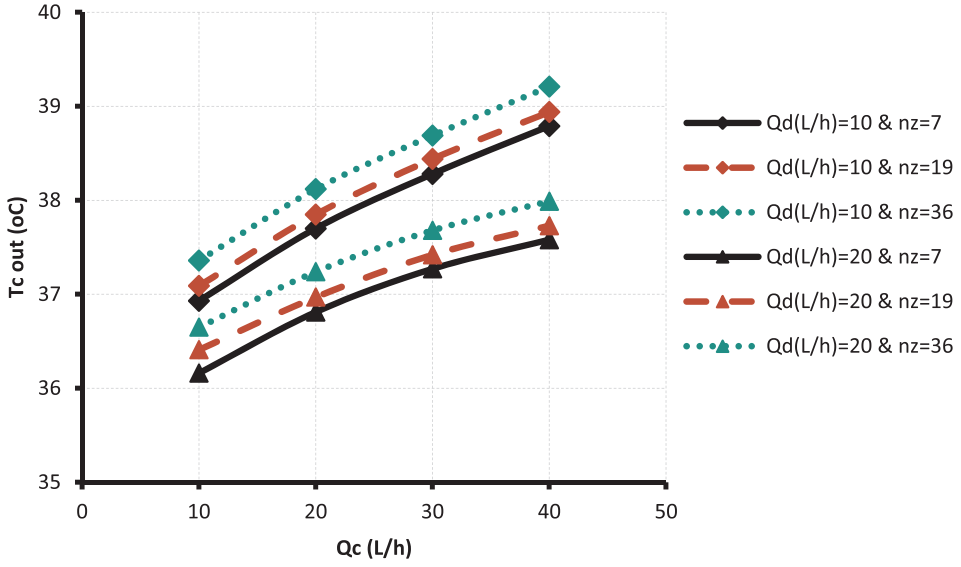

Fig. 6. The effect of the sparger configuration on the continuous phase outlet temperature for two different dispersed phase flow rates and three different nozzles number with constant nozzle diameter (D_z = 0.001 m).

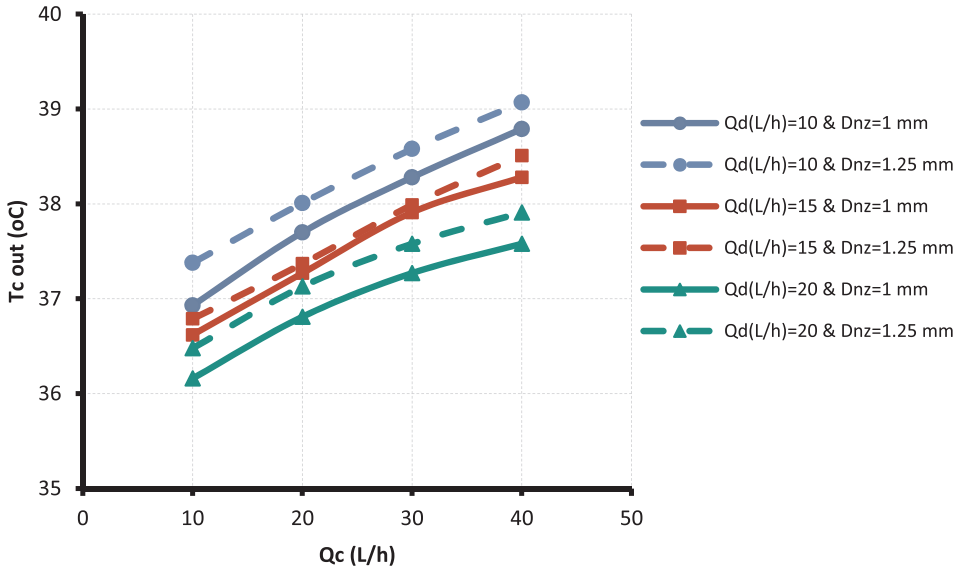

Fig. 7. The effect of diameter of injection nozzle in the sparger on the continuous phase outlet temperature for two different dispersed phase flow rates (nz = 7).

in the sparger.

The effect of the temperature driving force in terms of the Jakobs number (*Ja*) on the outlet temperature of the continuous phase is shown in Fig. 9. The figure presents three different sparger configurations, including the effect of the dispersed phase flow rate. It is demonstrated that the outlet temperature of the continuous phase increases with the *Ja* increase. However, this relationship seems linear, with no noticeable effect of the dispersed phase flow rate. Such behaviour of the outlet temperature of the continuous phase could be interpreted to indicate that, within the present experiment's conditions, further energy content is still available in the continuous phase, over and above what is required to achieve complete evaporation of the dispersed phase. This is clearly shown during the measurement of the height of complete evaporation of the drops in the heat exchanger [23]. Also, this is in agreement with the effect of the dispersed phase on the outlet temperature of the continuous phase which is shown in the same figure.

5. Conclusions

An experimental and analytical investigation of the temperature distribution along a liquid-liquid-vapour three-phase direct contact heat exchanger was carried out. In this investigation, the effects of many parameters, such as flow rates, nozzle configurations and continuous initial temperature distribution were studied. According to the results, it is concluded that the temperature of the dispersed phase increases with heat exchanger height, whereas it decreases for the continuous phase, regardless of the direction of the flow of phases. Flow rates of both the contacting phases affect the energy content of the continuous phase outlet in an opposite manner. An increase in the continuous phase flow rate results in an increase in the continuous phase outlet temperature, while the opposite is true for the dispersed phase. Interestingly, increases in the number of nozzles in the sparger and in the initial temperature of the continuous phase could lead to a reduction in the continuous phase flow rate and hence to a reduction in pumping costs.

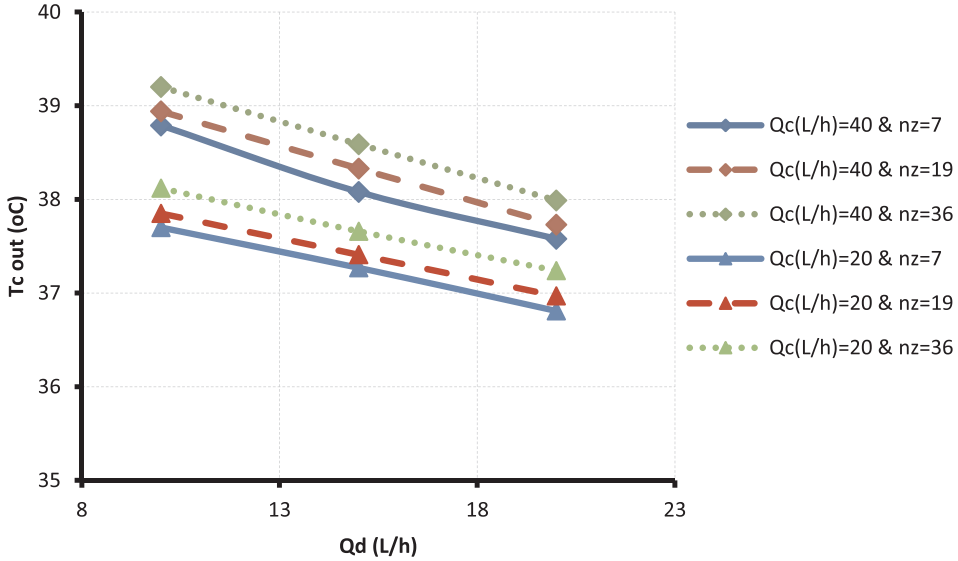

Fig. 8. The variation of the outlet temperature of the continuous phase with dispersed phase flow rate for different continuous phase flow rate and sparger configuration.

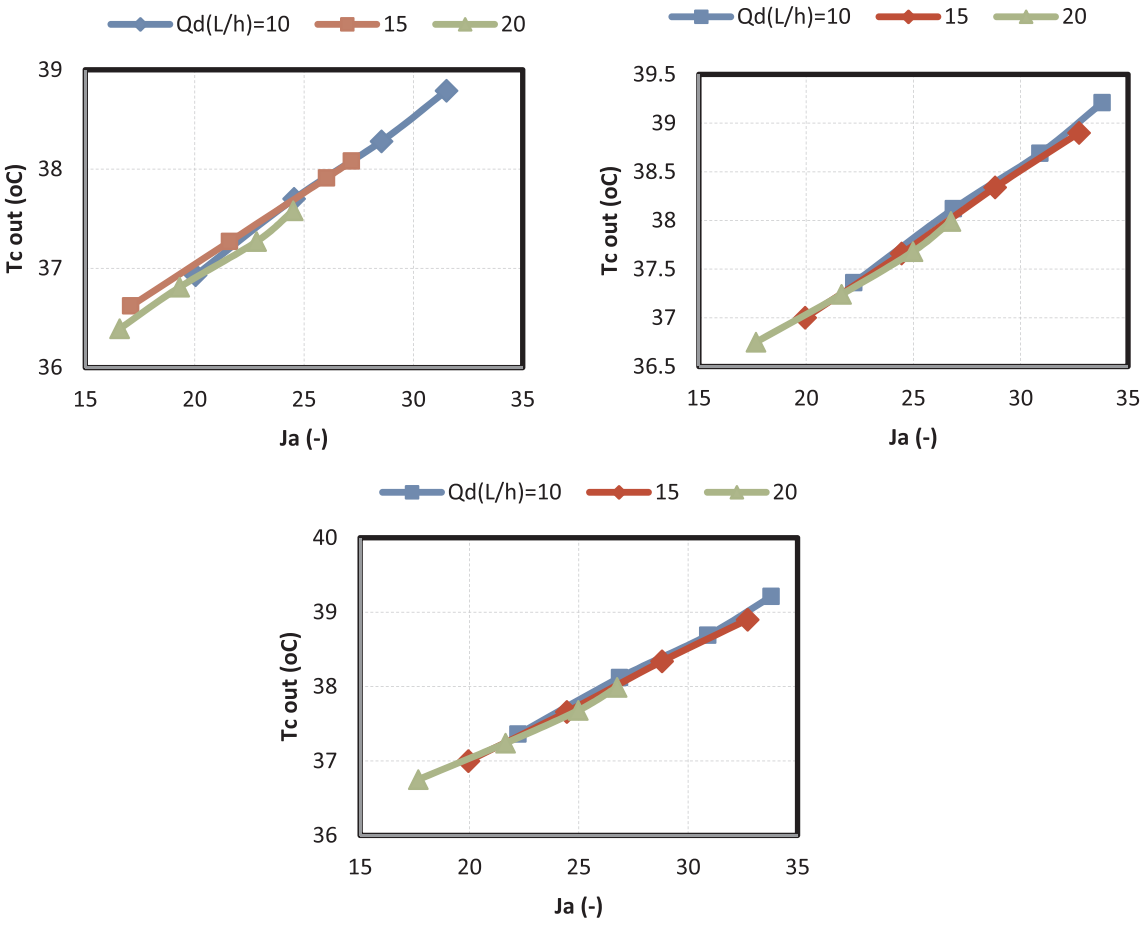

Fig. 9. The effect of Ja on the outlet temperature of the continuous phase.

References

[1] A.Sh. Baqir, H.B. Mahood, M.S. Hameed, Heat transfer measurement in a three-phase spray column direct contact heat exchanger for utilisation in energy recovery from low-grade sources, Energy Conv. Mang. 126 (2016) 342–351.

[2] H.B. Mahood, A.N. Campbell, R.B. Thorpe, A.O. Sharif, Heat transfer efficiency and capital cost evaluation of a three-phase direct contact heat exchanger for the utilisation of low-grade energy sources, Energy Conv. Manage. 106 (2015) 101–109.

[3] H.B. Mahood, Experimental and Theoretical Investigation of a Three-Phase Direct Contact Condenser, PhD Thesis Dep. of Chemical and Process Engineering, University of Surrey, UK, 2016.

[4] H.B. Mahood, Direct-contact heat transfer of a single volatile liquid drop evaporation in an immiscible liquid, Desalination 222 (1) (2008) 656–665.

[5] A. Gulevich, P. Martynov, V. Gulevsky, V. Ulyanov, Technologies for hydrogen production based on direct contact of gaseous hydrocarbons and evaporated water with molten Pb or Pb–Bi, Energy Conv. Mang. 49 (2008) 1946–1950.

[6] N.E. Wijeysundera, M.N. Hawlader, C.W. Andy, M.K. Hossain, Ice-slurry production using direct contact heat transfer, Int. J. Refrig. 27 (2004) 511–519.

[7] T. Kiatsiriroat, S. Vithayasai, N. Vorayos, A. Nuntaphan, Heat transfer prediction for a direct contact ice thermal energy storage, Energy Conv. Mang. 44 (4) (2003) 497–508.

[8] P. Battya, V.R. Raghavan, K.N. Seetharamu, Parametric analysis of direct contact sensible heat transfer in spray column, Lett. Heat Mass Trans. 9 (4) (1982) 265–276.

[9] T. Coban, R.F. Boehm, Performance of a three-phase, spray-column, direct-contact heat exchanger, J. Heat Transfer 111 (1) (1989) 166–172.

[10] H.R. Jacobs, M. Golafshani, A heuristic evaluation of the governing mode of heat transfer in a liquid–liquid spray column, J. Heat Transfer 111 (3) (1989) 773–779.

[11] K.L. Core, J.C. Mulligan, Heat transfer and population characteristics of dispersed evaporating droplets, AIChE J. 36 (8) (1990) 1137–1144.

[12] S.M. Summers, C.T. Crowe, One-dimensional numerical model for a spray column heat exchanger, AIChE J. 37 (11) (1991) 1673–1679.

[13] L. Tadrist, J. Sun, R. Santini, J. Pantaloni, Heat transfer with vaporization of a liquid by direct contact in another immiscible liquid: experimental and numerical study, J. Heat Transfer 113 (3) (1991) 705–713.

[14] R.A. Brickman, R.F. Boehm, Maximizing three-phase direct-contact heat exchanger output, Numer. Heat Transfer, Part A Appl. 26 (3) (1994) 287–299.

[15] H.B. Mahood, A.O. Sharif, S. Al-aibi, D. Hwakis, T.B. Thorpe, Analytical solution and experimental measurements for temperatures distribution prediction of three-phase direct contact condenser, Energy 67 (2014) 538–547.

[16] H.B. Mahood, A.O. Sharif, S.A. Hossini, R.B. Thorpe, Analytical modelling of a spray column three-phase direct contact heat exchanger, ISRN Chem. Eng. (2013), http://dx.doi.org/10.1155/2013/457805 457805.

[17] H.B. Mahood, R.B. Thorpe, A.N. Campbell, A.O. Sharif, Experimental measurements and theoretical prediction for the transient characteristic of a three-phase direct contact condenser, Appl. Therm. Eng. 87 (2015) 161–174.

[18] H.B. Mahood, A.O. Sharif, R.B. Thorpe, Transient volumetric heat transfer coefficient prediction of a three-phase direct contact condenser, J. Heat Mass Transf. 51 (2) (2015) 165–170.

[19] H.B. Mahood, A.N. Campbell, R.B. Thorpe, A.O. Sharif, Experimental measurements and theoretical prediction for the volumetric heat transfer coefficient of a three-phase direct contact condenser, Int. Comm. Heat Mass Trans. 66 (2015) 180–188.

[20] H.b. Mahood, A.N. Campell, A.O. Sharif, R.B. Thorpe, Heat transfer measurement in a three-phase direct contact condenser under flooding conditions, Appl. Therm. Eng. 95 (2016) 106–14.

[21] H.B. Mahood, A.O. Sharif, R.B. Thorpe, A.N. Campbell, Heat transfer measurements of a three-phase direct contact condenser for application in energy production and water desalination, in: The 3rd Int Conf on Water, Energy and Env, Sharjah, Aus, 24–27 March 2015.

[22] H.B. Mahood, A.N. Campbell, R.B. Thorpe, A.O. Sharif, Measuring the overall volumetric heat transfer coefficient in a vapor-liquid–liquid three-phase direct contact heat exchanger, Heat Trans. Eng. < http://dx.doi.org/10.1080/01457632.2017.1295736 > .

[23] A.Sh. Baqir, H.B. Mahood, A.N. Campbell, A.J. Griffiths, Measuring the average volumetric heat transfer coefficient of a liquid-liquid-vapour direct contact heat exchanger, Appl. Therm. Eng. 103 (2016) 47–55.

[24] H.B. Mahood, A.N. Campbell, R.B. Thorpe, A.O. Sharif, A new model for the drag coefficient of a swarm of condensing vapour-liquid bubbles in a third immiscible liquid phase, Chem. Eng. Sci. 131 (2015) 76–83.

[25] H.B. Mahood, A.O. Sharif, S. Al-aibi, S.A. Hosssini, R.B. Thorpe, Heat transfer modelling of two-phase bubbles swarm condensing in three-phase direct contact condenser, J. Therm. Sci. 20 (1) (2016) 143–153.

[26] R. Wanchoo, S. Sharma, G. Raina, Drag coefficient and velocity of rise of a single collapsing two-phase bubbler, AIChE J. 43 (8) (1997) 1955–1963.

[27] J. Isenberg, S. Sideman, Direct contact heat transfer with change of phase: bubble condensation in immiscible liquids, Int. J. Heat Mass Transf. 13 (6) (1970) 997–1011.

[28] D. Moalem, S. Sideman, A. Orell, G. Hetsroni, Direct contact heat transfer with change of phase: condensation of a bubble train, Int. J. Heat Mass Transf. 16 (12) (1973) 2305–2319.

[29] D. Moalem, M. Sokolov, S. Sideman, A closed periodic condensation-evaporation cycle of an immiscible, gravity driven bubble, Int. J. Heat Mass Transf. 23 (11) (1980) 1417–1424.

[30] S. Sideman, G. Hirsch, Y. Gat, Direct contact heat transfer with change phase: effect of the initial drop size in three-phase heat exchanger, AIChE J. 11 (6) (1965) 1081–1087.